Article

Not peer-reviewed version

Correlation Between Molecular Genetic Analysis and Nuclear Pleomorphism in Long-Term Recurrent and Metastatic Chordoma

Sarah Rebecca Ullmann , Julian Schreier , Joana Maria Ullmann , Marilena Georgiades , Christoph Hubertus Lohmann , Martin Röpke , Denny Schanze , Juan Carlos Alberto Uribe Caputi , Sabine Franke , Franziska Sabrina Karras , Albert Roessner *

Posted Date: 3 February 2026

doi: 10.20944/preprints202602.0214.v1

Keywords: chordoma; recurrences; metastases; nuclear morphometry; TMB; WES; immunohistochemistry

 doi:10.20944/preprints202602.0214.v1

Article

Correlation Between Molecular Genetic Analysis and Nuclear Pleomorphism in Long-Term Recurrent and Metastatic Chordoma

Sarah Rebecca Ullmann [1], Julian Schreier [1], Joana Maria Ullmann [2], Marilena Georgiades [3], Christoph H. Lohmann [4], Martin Röpke [4], Denny Schanze [5], Juan Carlos Alberto Uribe Caputi [6], Sabine Franke [1] Franziska Karras [1] and Albert Roessner [1,] *

[1] Institute of Pathology, Otto-von-Guericke University, Magdeburg, Germany; sarah.ullmann@ovgu.de
[2] Institute of Pathology, University Medical Centre Rostock, Rostock, Germany
[3] University Clinic for Radiology and Nuclear Medicine, Otto-von-Guericke University, Magdeburg, Germany
[4] University Orthopedic Clinic, Otto-von-Guericke University, Magdeburg, Germany
[5] Institute of Human Genetics, Otto-von-Guericke University, Magdeburg, Germany
[6] Universidad Autónoma de Bucaramanga UNAB, Molecular Immunology and Epidemiology, Bucaramanga, Colombia
* Correspondence: albert.roessner@med.ovgu.de

Simple Summary

Chordomas are rare malignant tumors with high recurrence rates and scarce treatment options due to the chemo- and radiation insensitivity. To date, it is difficult to predict which tumors are likely to recur, because routine light microscopy and imaging do not reliably capture subtle biological changes. We measured tumor cell nuclei in primary tumors, long-term recurrences and metastases using quantitative image-based methods and compared the results with protein expression and genome-wide mutation load obtained from whole exome sequencing. Recurrent tumors showed measurable pleomorphic changes and higher proliferation over time. Loss and disruption of key nuclear envelope proteins in highly irregular nuclei could be observed in recurrences and metastases. These results suggest that objective nuclear measurements, combined with molecular profiling may help identify aggressive disease course and provide a foundation for the development of automated digital AI-assisted tools for future risk assessment.

Abstract

Background/Objectives: Recurrences and metastases occur frequently in chordoma and are the main influence on overall survival. However, prognostic biomarkers for recurrence remain limited. This study examines whether quantitative nuclear morphometry captures recurrence evolution and whether it aligns with immunophenotype and genomic profiling. **Methods**: 26 specimens from 12 adults (eight non-recurrent tumors and four patients with multiple long-term recurrences and metastases over seven to sixteen years) were analyzed using whole-exome-sequencing, immunohistochemistry and nuclear morphometry. **Results**: Imaging studies and routine histology showed no consistent differences between groups. Morphometry revealed substantial intertumoral variability among non-recurrent tumors and significant longitudinal nuclear remodeling throughout recurrences, dominated by increased nuclear size and asymmetry as well as altered shape. Primary tumors from patients who later recurred had smaller, more asymmetric and denser nuclei than non-recurrent tumors. Recurrent samples showed higher proliferation and decreased lamin A/C expression with focal disruption and detachment from the nuclear envelope in pleomorphic nuclei. The tumor mutational burden was overall low, varied between patients and timepoints and tended to be higher in recurrent cases. **Conclusions**: Quantitative nuclear morphometry, integrated with

 doi:10.20944/preprints202602.0214.v1

immunophenotyping and genomic profiling captures recurrence-associated phenotypic remodeling in chordoma and may support/train future AI-models for risk stratification.

Keywords: chordoma; recurrences; metastases; nuclear morphometry; TMB; WES; immunohistochemistry

1. Introduction

Chordomas are rare malignant bone tumors mostly affecting the axial skeleton and skull base [1]. The tumorigenesis of chordoma remains incompletely understood, though they are presumed to originate from undifferentiated remnants of notochordal cells in adults or develop from a benign notochordal cell tumor (BNCT) [2]. Histologically, chordomas are classified as conventional, dedifferentiated or poorly differentiated [3]. Conventional chordomas are typically comprised of physaliphorus cells within a myxoid stroma and arranged in lobules separated by fibrous septa [4]. Some tumors exhibit necrosis, hemorrhage or BNCT-like components [5]. Although chordomas are slow growing and could biologically be considered low-grade tumors [6], they can be compared to sarcomas in point of aggressiveness due to their high local recurrence rate of 65% and risk of metastasis [7].

Pleomorphic changes in form and structure of nuclei and nucleoli as well as tissue architecture can be characteristic of tumor progression or recurrence in solid tumors [8] and have been recognized as a key criterion for tumor grading [9] though qualitative assessments often show a high interobserver variability [10]. Consequently, the quantitative analysis of histopathological findings was established as a complementary diagnostic tool in numerous malignancies [10,11], including breast cancer [12], urothelial neoplasms [13–15], malignant melanoma [16], colorectal cancer [17], myxoid liposarcoma [18] and mantle cell lymphoma [19]. Morphometry was successfully used for the differentiation between benign and malignant thyroid lesions [20]. Several studies have evaluated nuclear dysregulation in recurrences or metastases across other solid tumors [21]. A change of histological grade based on nuclear morphometry has been observed in locally recurrent soft tissue sarcomas [22]. Furthermore, nuclear morphometry has been applied to predict recurrence in osteosarcoma [23] and ductal carcinoma in situ of the breast [24] as well as in the differentiation between primary and metastatic lesions in Wilms' tumors [25]. However, no dedicated morphometric studies on recurrent chordoma have been published although nuclear pleomorphism has been discussed as a prognostic factor in conventional chordoma [26,27].

Histological abnormalities are central criterions for histopathological diagnosis of malignancy [28], taking size, shape, chromatin structure and irregularities of the outer nuclear membrane into consideration [29,30]. However, investigations rarely integrate morphological abnormalities with molecular genetic alterations [20,31]. Sarcomas generally exhibit a lower tumor mutational burden (TMB) compared with other carcinomas [32]. Furthermore, carcinomas can show considerable genomic evolution in recurrences and metastases [33]. In contrast little is known about the long-term genomic evolution of other mesodermal tumors such as chordomas [34,35]. Specifically, it remains unclear whether the tumor mutational burden (TMB) and other measures of mutational accumulation are associated with reproducible changes in nuclear morphometry and immunophenotype in recurrent chordoma [36].

This study investigates the association between histological and immunohistochemical findings, quantitative nuclear pleomorphism and molecular measures of tumor mutational load, particularly the TMB in long-term recurrent versus non-recurrent chordomas.

The objective is to characterize morphometric, immunophenotypic and molecular evolution over time, through the relationship between morphonuclear alterations and genetic developments, thereby contributing to a more comprehensive understanding of recurrence development in chordoma. These findings are expected to provide some insights into therapeutic options and inform future studies on therapeutic vulnerabilities in long-term recurrent chordoma.

 doi:10.20944/preprints202602.0214.v1

2. Materials and Methods

2.1. Sample Selection

This is a descriptive case series study of tissue samples from patients with non-recurrent chordomas and those with multiple long-term recurrences and/or metastases, in whom histological features, immunohistochemical profiles, nuclear pleomorphism and TMB were evaluated. A total of 26 formalin-fixed, paraffin-embedded (FFPE) tissue samples from 12 patients were retrieved from the histopathological archives of the bone tumor registry of the Institute of Pathology of the Otto-von-Guericke University, Magdeburg, Germany. Of the 12 patients, eight had primary tumors without recurrences, whereas four developed multiple long-term recurrences and/or metastases. Additional clinical data were provided by the Departments of Orthopedic Surgery and Radiotherapy. The clinical data, summarized in Figure 1, included age, sex, tumor site, treatment regimens (radio-/chemotherapy) and the timing of long-term recurrences where available. This study was approved by the Ethics Committee of the Medical Faculty of the Otto-von-Guericke-University of Magdeburg, Germany (Approval No. 132/21) and informed consent was obtained from all patients.

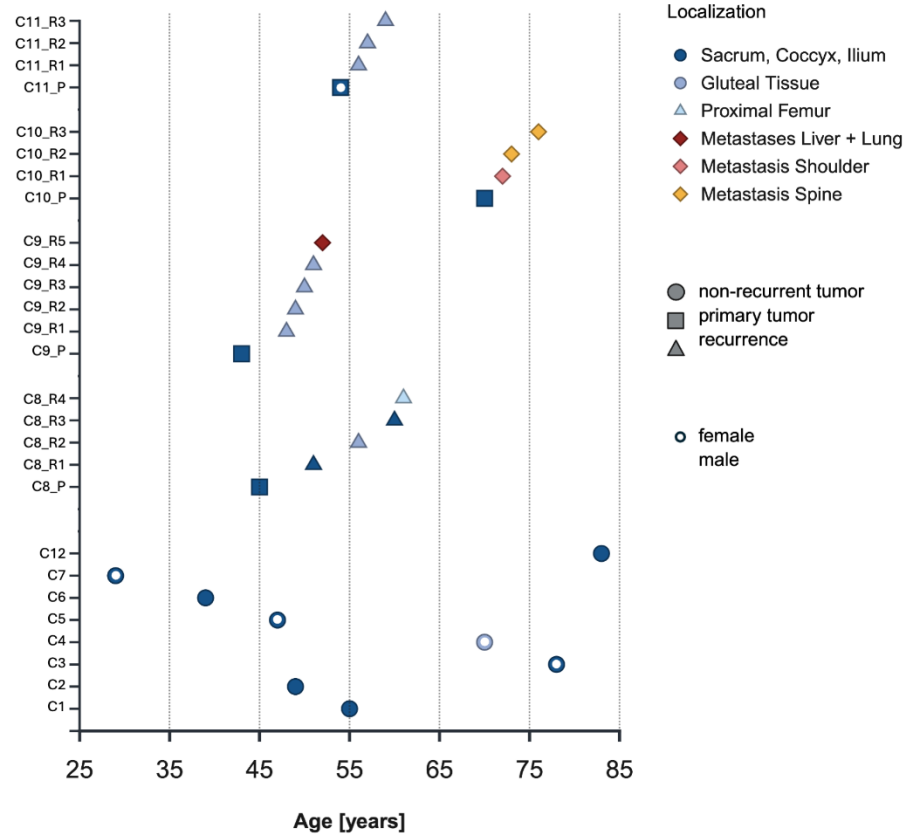

Figure 1. Clinical information for all patients is visualized over time with the color of the data point representing the localization of the tumor. Cn = case number, Rn recurrence number. Patients with non-recurrent tumors have a heterogeneous age distribution with a mean age of 52 ±18.61 years. Patients that would develop multiple long-term recurrences were 53 ±12.30 years old at the time of diagnosis and had 3.5 recurrences on average over a time span of seven to 16 years.

2.2. Histopathological Analysis

An experienced bone pathologist (A.R.) reviewed all slides, evaluated the histology and classified the tumors according to the current WHO classification of Tumors of Soft Tissue and Bone (5th edition). Only conventional sacral chordomas in adult patients were included in this study.

 doi:10.20944/preprints202602.0214.v1

2.3. Immunohistochemistry

Immunohistochemical staining was performed on all samples for brachyury (EPR18113, Abcam limited, UK), Ki-67 (MIB-1, Dako Corporation, Agilent, CA, USA), p53 (453M-95, DO7, Cell Marque, Rocklin, CA, USA), S100 (Z0331, Dako Corporation, Agilent), Vimentin (Vim384, Dako Corporation, Agilent), E-Cadherin (EP700Y, Cell Marque, Darmstadt, Germany), Pancytokeratine (PCK, AE1/3, Leica Biosystems, Germany), EGFR (E30, Dako Corporation, Agilent), VEGF (VG-1, Santa Cruz Biotechnology, Texas, USA), SMARCB1 (25/BAF47, BD Biosciences, New Jersey, USA), Lamin A/C (EP4520-16, Abcam Cambridge Biomedical Campus, UK), PD-1 (315M-95, Cell Marque, Rocklin, CA, USA) and PD-L1 (M3653, Dako Corporation, Agilent). Formalin-fixed, paraffin-embedded (FFPE) tissue sections (2µm) were dewaxed in xylene and rehydrated through graded ethanol, followed by antigen retrieval using EDTA buffer (1 mM; pH and retrieval conditions according to the laboratory standard protocol). Staining was performed using the automated immunohistochemistry slide staining system by Ventana NexES (Ventana Medical System, Darmstadt, Germany). Sections were incubated with the respective primary antibodies at 37 °C for 30 min. The Ki-67-Index was determined by manual counting in 2-6 randomly selected high-power fields per slide (400x), expressed as the percentage of positively stained tumor nuclei. On average 1,764 nuclei were analyzed per sample (44,107 nuclei in total).

The p53 index was determined analogously by manual counting in one randomly selected field per slide (200x), expressed as the percentage of tumor nuclei with strong staining. In total 24,478 nuclei were counted (mean 1,064 per sample).

2.4. Morphometry

Nuclear morphometry was assessed by measuring a mean of 317 ± 15 nuclei per sample on H&E-stained slides at 600x magnification using NIS Elements D Software, (Nikon Instruments Inc, Melville, NY, USA; v4.20.03). Nuclei were manually traced on digitally captured images using a mouse and results were tabulated in Excel. In addition to nuclear area, further morphometric parameters were assessed to characterize differences in nuclear features between non-recurrent cases and recurrent/metastatic disease courses. These included size, shape, texture, and density descriptors. The methodological framework was adapted from Khatri et al., who used morphometric analysis to distinguish between benign and malignant thyroid lesions [20].

2.5. Whole Exome Sequencing

Whole exome sequencing (WES) widely used for determining TMB and provides broad genomic coverage compared with targeted panels [37,38]. TMB is commonly defined as the number of non-synonymous somatic variants per megabase of callable coding sequence [39]. Consequently, the mutational profiles in this cohort were analyzed through WES.

Prior to DNA-extraction, tumor areas were marked on 2 µm H&E-stained FFPE slide by an experienced pathologist and traced on 6 µm slides under 100x magnification via VWR VisiScope-Microscope. Marked tissue was macrodissected prior to deparaffination following the standardized protocol of the laboratory for molecular diagnostics of the institute for pathology in Magdeburg, Germany. Subsequently DNA was isolated using the NucleoSpin® Tissue DNA purification kit from Machery-Nagel GmbH, Düren, Germany, following the manufacturer's instructions. Extracted DNA was quantified using a Qubit Fluorometer (Invitrogen Thermo Scientific by life technologies, Oregon, USA), with the Qubit™ dsDNA HS Assay Kit and stored at -20°C. The SureSelect XT HS2 DNA System for DNA library preparation and target enrichment for the Illumina platform from Agilent Technologies (Santa Clara, CA, USA) was used for enzymatic fragmentation, library preparation and hybridization and capture as well as post-capture sample processing for multiplex sequencing following the manufacturers protocol version D0 from April 2021. DNA-quality and quantity were assessed regularly between workflow steps. Captured libraries were stored at -20°C before

 doi:10.20944/preprints202602.0214.v1

sequencing on an Illumina NextSeq®550) at the Institute for Human Genetics of the University Hospital Magdeburg, Germany (Medical Faculty, Otto-von-Guericke University).

The sequenced data was processed through the varvis®-pipeline (varvis variant analysis v1.21.2, limbus-medtec, Rostock, Germany) [40] and aligned to the GRCh37 reference genome for variant calling applying the following filters: Minor allele frequency (MAF) Gnom total of under 0.001, variant allele frequency (VAF) of ≥ 0.1, reads-index ≥ 40, impact "high" or "moderate" (as annotated by varvis) and a AltAF-Index ≥ 0.15 to reduce low-level subclonal calls. Amino acid changes that did not alter the protein-product (synonymous variants) were excluded. Putative germline polymorphisms were filtered using dbSNP and the internal varvis database. Variants observed in ≥100 entries in the internal database were excludet (AllexesFound ≥ 100). TMB was calculated as SNVs+InDels per 35 megabases.

2.6. Statistical Analysis

All statistical analyses were performed using MATLAB (The MathWorks Inc. v9.9/R2020b) and Microsoft Excel (Microsoft Corporation, v16.95.4 (25040241)). The Shapiro-Wilk test was used to assess normality, supported by visual inspection of individual histograms and Q-Q plots. Variance homogeneity was assessed using Levene's test and visualized through boxplots. The Kruskal-Wallis test, a non-parametric method robust to unequal variances, was chosen to compare non-recurrent tumors as independent data points. Changes within recurrent cases were treated as dependent measurements and analyzed using the Friedman test due to the absence of normal distribution. A Bonferroni correction was applied to control the family-wise error rate. The Mann-Whitney-U test was employed to compare non-recurrent tumors (NRTs) with primary tumors from recurrent cases. Results were visualized using violin plots.

Morphometric features were grouped into four categories: size (nuclear area, equivalent diameter, circumference, nuclear area coefficient of variation), shape (formfactor, Feret diameters), texture (roughness) and density (density, intensity, brightness).

In measurements of nuclear size, nuclear area and circumference are directly measured, providing a simplified size approximation that disregards shape. The nuclear area coefficient of variation (NACV) was calculated as: $\left(\frac{SD\ of\ nuclear\ area}{mean\ nuclear\ area}\right) \times 100$.

Shape parameters include the formfactor, minimal and maximum Feret diameters as well as the maximum Feret diameter measured at 90° rotation (maxFeret90). The formfactor quantifies how closely an object approximates a perfect circle, with values approaching 1 indicating high circularity. It was calculated as: Formfactor = $\frac{(4\pi \times area)}{(circumference^2)}$. MinFeret and MaxFeret describe the shortest and longest distance between two parallel tangents applied to the nuclear contour, reflecting the maximum/minimal nuclear expansion. A high MaxFeret and low MinFeret suggests elongated or deformed nuclei [41]. MaxFeret90 refers to the maximal Feret diameter measured perpendicular to the original MaxFeret. The difference between MaxFeret and MaxFeret90 allows inference on object symmetry, with larger differences pointing to greater irregularity [42].

Density parameters include density and intensity or brightness. Sum intensity represents the total of all pixel intensity values within a selected region. Sum density (or integrated density) was defined as the cumulative density of all measured pixel values normalized by area accounting for spatial distribution: $SumDensity = \sum(pixel\ intensity \times pixel\ area)$. This allows for comparisons between nuclei of different sizes and enables conclusions about chromatin content. Denser chromatin packing or increased DNA content results in higher sum or mean density values, provided imaging conditions are standardized. To account for area differences, sum density was preferred over sum intensity in this analysis and images were captured with standardized microscope and camera settings.

Normality testing rejected the null hypothesis of normal distribution for all parameters. In comparison of non-recurring tumors, Levene's test showed strong evidence for heterogeneity of variances across NRTs for all measurements ($p < 0.001$). Given non-normal distribution and

 doi:10.20944/preprints202602.0214.v1

heteroscedasticity, the Kruskal-Wallis's test was employed as a non-parametric option to test whether medians across NRTs differed significantly.

3. Results

3.1. Clinical Data and Radiology

Clinical data for all patients are summarized in Figure 1. Patients with non-recurrent tumors showed a heterogeneous age distribution with a mean age of 56.25 ± 19.11 years. In the recurrent/metastatic group, patient 10 represented an outlier and was diagnosed at the age of 70, exceeding the median age of 47.33±5.9 of the other members of the recurrence group and raising the average age to 53.00 ±12.30 years. His case is further distinguished by the development of multiple metastases over a seven-year period involving the lumbar and thoracic spine as well as the coracoid process (Figure 2). The patient received systemic therapy with imatinib (2014 – 2016) and radiation therapy for distant metastases (shoulder/coracoid process and thoracic vertebrae) through 2018. Across the available imaging, no consistent imaging differences were observed between patients with recurrent/metastatic and non-recurrent chordomas.

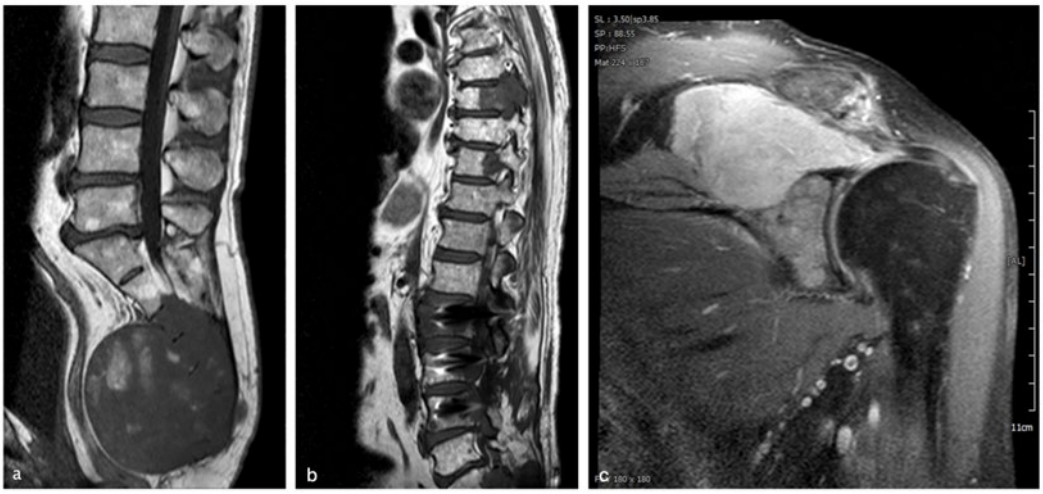

Figure 2. MRI of a 70-year-old patient with sacrococcygeal chordoma. The tumor exhibits low signal intensity on T1-weighted images (a), with small foci of hyperintensity indicative of intratumoral hemorrhage. Figure 2b shows the MRI of the same patient 7 years later after he presented with acute transverse lesion and received immediate radiation therapy. The sagittal T1 imaging plane shows two intraspinal lesions originating from TH6-TH8 with absolute spinal canal stenosis and possible infiltration of the myelon as well as size-progression in a previously known space-occupying lesion in the lumbar spine region. The T1/TSE coronal, fat suppressed imaging plane (c) with intravenous contrast documents a metastases in the processus coracoideus of the left shoulder with destruction of the glenoid, that was first diagnosed three years earlier but left untreated due to poor overall cardiovascular condition of the patient.

3.2. Histology

All tumors investigated in this study – both primary and recurrent - were conventional chordomas, with intralesional fibrous septa containing fibroblastic cells and collagen fibers as a typical defining morphologic feature [43]. Such septa were present to varying degrees in all samples. Overall, their share of tissue was relatively low. Estimated tumor purity exceeded 80% in all specimens. In most cases, the characteristic myxoid pattern predominated. This pattern is marked by abundant extracellular spaces that give the superficial impression of intracellular vacuoles - a phenomenon that originally led to the concept of "physaliphorus" cells [4]. The solid subtype of myxoid chordoma, as described by Naka et al. in 2003, was not encountered in our cohort [26]. A

 doi:10.20944/preprints202602.0214.v1

histological survey did not reveal any differences in the histological appearance between primary tumor and fourth recurrence in case eight after 16 years (Figure 3 a, b). The degree of nuclear pleomorphism appeared broadly comparable between primary tumors and recurrent samples (Figure 3 a, b). At high-power magnification, some nuclei of chordoma cells exhibited significant pleomorphism, which is a distinctive cytological characteristic of this tumor entity [26,27]. This pleomorphism was particularly evident when compared with nuclei of adjacent lymphocytes and fibroblasts (Figure 3 c). In some tumor areas pleomorphic nuclei with coarse chromatin were observed along with dents and folds in the membrane and detachment of heterochromatin from the nuclear envelope (Figure 3 d).

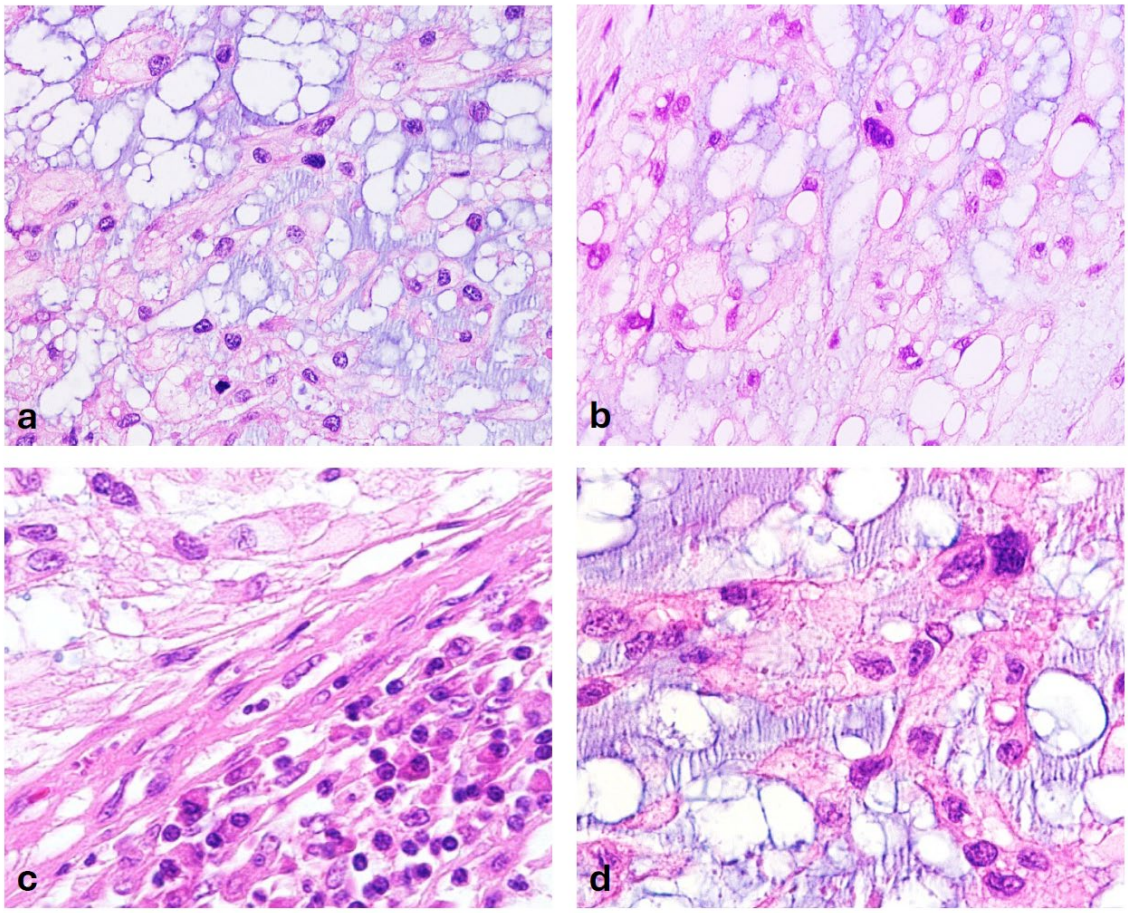

Figure 3. Primary tumor case 8. (a) Typical appearance of conventional chordoma with physaliphorus cells (H&E x400). (b) On histological grounds, no differences can be observed between primary and long-term recurrence after 16 years (H&E x400). (c) Enlarged tumor cell nuclei with irregular shape and prominent nucleoli (upper left corner) stand out in comparison to lymphocytes in the lower right corner with round, smaller nuclei as well as adjacent fibroblasts with regular, spindle shaped nuclei (H&E x 600). (d) Bundles of tumor cell nuclei with remarkably coarse chromatin and conspicuously irregular shape of the outer nuclear membrane with folds and dents as well as heterochromatin detached from nuclear membrane (H&E x800).

3.3. Immunohistochemistry

The immunohistochemical results are summarized in Figure 4. All samples stained positive for vimentin and cytokeratin AE1/3, with no observable differences in expression between primary tumors and recurrences. VEGF staining among NRT samples was heterogenous: 20% of samples were negative, 30% strongly positive, 50% moderately positive. Notably, case 10 showed weak VEGF expression in the primary tumor but no detectable expression in subsequent recurrences. EGFR showed a similar heterogenous pattern among NRTs. Sixty percent of NRTs stained positive for S100.

 doi:10.20944/preprints202602.0214.v1

In contrast, three of four recurrent cases demonstrated increasing expression of VEGF, EGFR and S100 over time. SMARCB1 loss has recently been associated with poorly differentiated chordomas [44,45] and a partial loss has been found in conventional chordomas [46]. Partial nuclear protein loss was observed in some NRTs in our cohort. However, SMARCB1 loss occurred in all recurrent cases, most notably in case 8 which had retained SMARCB1-expression in its primary tumor with a subsequent progressive loss. All samples stained positively for brachyury.

The Ki-67 proliferation index increased from primary tumors to last recurrences by a mean of 5.9 % ± 4.4 (Figure 5 a, b). The proliferation indices in the NRT group (4.6 % ± 3.5) were lower than in recurrent samples. The Ki-67 index in primary tumors of recurrence cases (4.1% ± 3.7) was comparable to that of NRTs, but proliferation increased markedly in the recurrences. p53 immunoreactivity was variable and positive nuclei were observed in approximately half of NRT samples and recurrent cases. Case 8 exhibited an increased staining intensity over time, whereas case 10 lost p53 expression. As depicted in Figure 5 c, d and Table 2, p53 positivity was generally lower in primary tumors (<1%) than in recurrences (>10%).

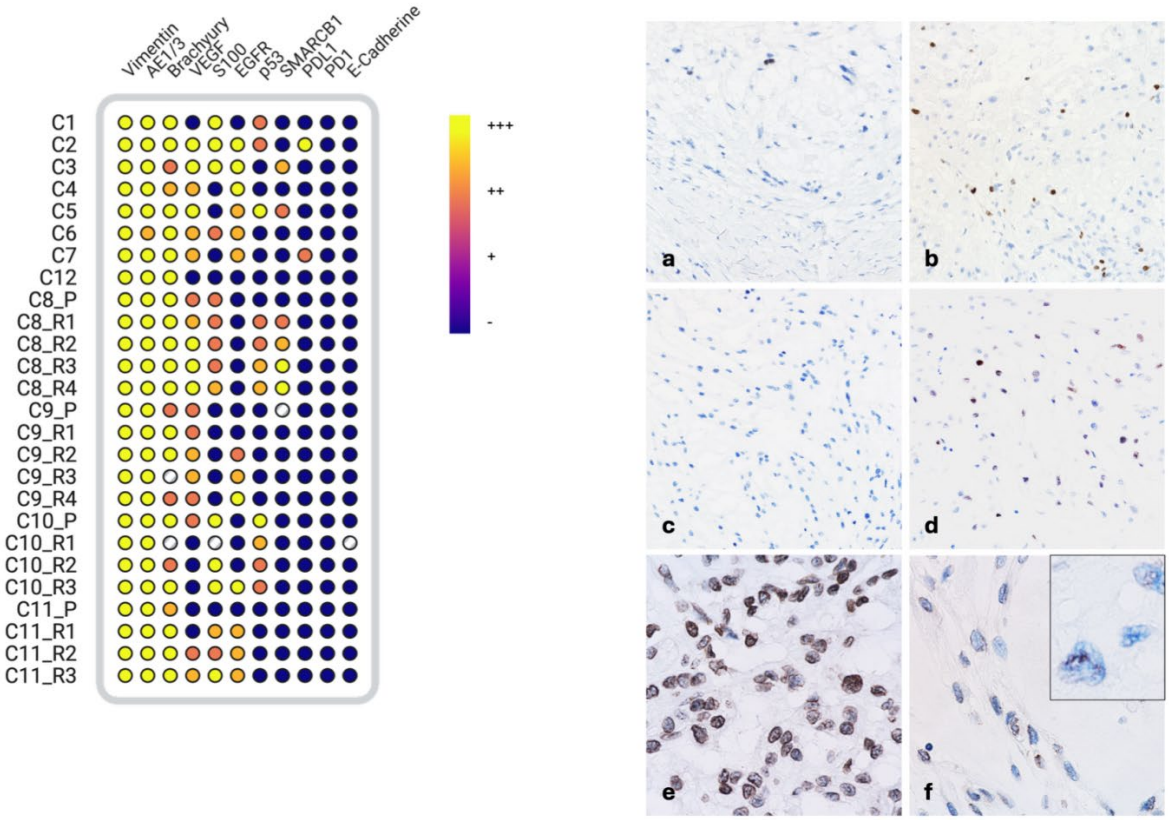

Figure 4. (left). Wellplate heatmap of all immunohistochemical results categorized into strongly positive staining (+++), positive staining (++), slightly positive staining (+), negative staining (-). Wells without color represent samples with methodical difficulties in staining. **Figure 5 (right).** (a) Low Ki-67 expression index in the primary tumor of case eight (200x). (b) High index in the fourth recurrence after 16 years (200x). (c) Occasional p53 positive nuclei in the primary tumor (200x). (d) Higher p53 expression in the last recurrence. (e) Strong expression of lamin A/C at the nuclear envelope of nuclei from the primary tumor (400x). (f) Decreased lamin A/C staining in pleomorphic nuclei after 16 years. Spatial disintegration of lamin A/C can be observed (inset 600x).

Lamin A/C staining demonstrates a strong expression at the nuclear envelope of non-recurrent tumors and the primary tumor of case 8 (Figure 5 e). In the fourth recurrence after 16 years, only part of the nuclei were stained with considerably lower intensity (Figure 5 f). Furthermore, pleomorphic

 doi:10.20944/preprints202602.0214.v1

nuclei in the last recurrence revealed spatial disintegration of the lamin A/C component with only lamin-remnants remaining in the nuclear envelope (Figure 5 f inset 600x).

3.4. Morphometry

NRTs displayed a heterogeneous distribution, with most samples showing significant differences in median values for size and density parameters (Figure 6). Shape parameters showed a similar pattern, apart from the formfactor, for which 39% of comparisons did not show significant differences. For nuclear area, equivalent diameter, MinFeret, MaxFeret and MaxFeret90, 82% of comparisons differed significantly. This proportion was even higher for circumference and density (89%). To assess nuclear symmetry, the difference between MaxFeret and MaxFeret90 was calculated (ΔFeret = MaxFeret – MaxFeret90). While no statistically significant differences in ΔFeret were found among NRTs, a slight but nonsignificant trend toward increased asymmetry was observed.

For recurrent cases the Friedman test with Bonferroni-adjusted post hoc comparisons was applied to determine whether significant changes occurred over time.

Preprints.org (www.preprints.org) | NOT PEER-REVIEWED | Posted: 3 February 2026 doi:10.20944/preprints202602.0214.v1

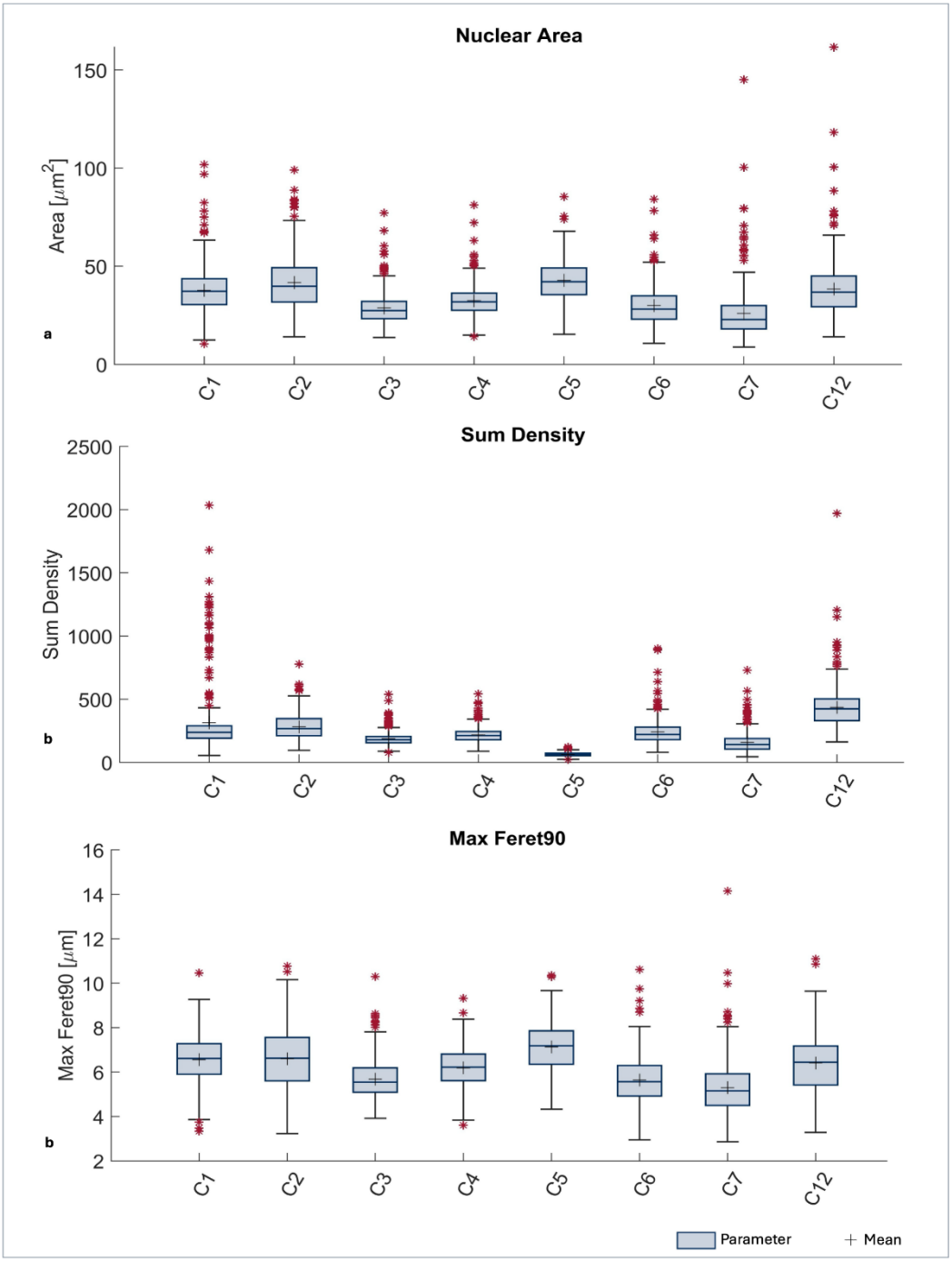

Figure 6. Boxplots of nuclear area as an example for size parameters (a), maxferet90 for shape parameters (b) and density (c) all show a heterogenous distribution of measurements of tumors without recurrences.

Case 8 showed highly significant changes ($p < 0.001$) in size and density parameters (nuclear area, equivalent diameter, circumference) with the exception of the second vs. third recurrence, which did not differ in area or diameter (Figure 7 a). All density measurements differed significantly (Figure 7b). Furthermore, MaxFeret and formfactor also changed significantly, while MinFeret and MaxFeret90 only showed significant change between the first and second recurrence (Figure 7c). Case 9 demonstrated similar results, with significant differences across all size parameters omitting the transition in circumference from third to fourth recurrence ($p = 0.299$) (Figure 7a). Shape parameters again yielded analogous results except for MaxFeret between the third and fourth recurrence (Figure 7c). Case 10, which stood out clinically due to hematogenous metastasis, presented significant changes in all parameters regarding size and density (Figure 7a, b). Three exceptions were noted

 doi:10.20944/preprints202602.0214.v1

among shape parameters: MinFeret (p = 0.435) and MaxFeret90 (p = 0.715) between the first and second recurrence and formfactor between the second and third recurrence (Figure 7c).

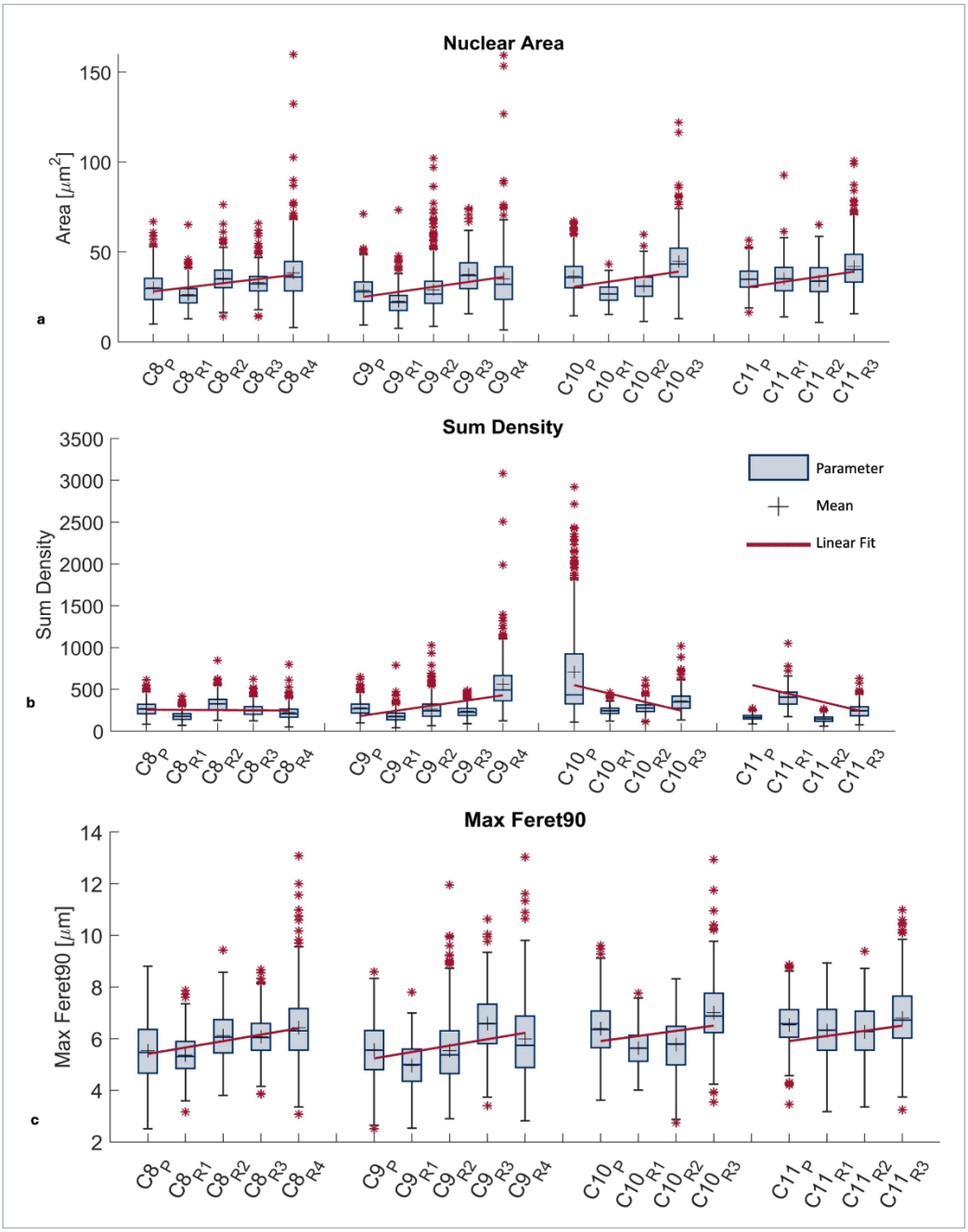

Figure 7. Boxpolots with linear fit of nuclear area as a size parameter (a), of density (b) and shape (c) parameters in recurrent cases. Most patients show a highly significant increase over time in size as well as in all ferret measurements indicating increasing deviances in shape. Within samples of density (b) no trend over time could be observed.

Contrary to these results, case 11 offers solely nonsignificant findings for all size parameters (Figure 7a) and only some significant developments involving the formfactor (primary tumor vs. first recurrence), and MinFeret, MaxFeret and MaxFeret90 (second vs. third recurrence) (Figure 7c). Interestingly, sum density differed significantly across all samples in this case (Figure 7b).

Texture parameters (roughness) and additional density measures showed no consistent trends or significant differences between NRTs and recurrent cases, nor over time within recurrences.

 doi:10.20944/preprints202602.0214.v1

Finally, the Mann-Whitney U test was used to compare primary tumors from patients who later recurred with NRTs, after confirmation of variance heterogeneity via Levene's test. All size parameters differed significantly between both groups. Congruent results could be observed for density and MinFeret, MaxFeret90 and formfactor. Only MaxFeret did not allow rejection of the null hypothesis (p = 0,934). Table 1 summarizes group values and p-values of both groups. Primary tumors of recurrence cases had slightly smaller nuclei, greater deviation from circular shape, and higher nuclear density than non-recurrent tumors. As noted above, these differences were not apparent on qualitative histologic assessment of H&E slides.

Table 1. Mean measurements ± standard deviation for pleomorphic parameters in non-recurrent tumors and primary tumors of recurrent cases. A p-value of <0.05 was considered statistically significant. Parameters for size and density as well es all formfactor and MinFeret and MaxFeret90 differed significantly between both groups.

Nuclear Parameter	NRTs (n=2553)	Primary Tumors of RCs (n=1256)	p-value (Mann-Whitney-U)
Nuclear Area [µm²]	34.893 ± 13.274	32.268 ± 10.521	0.0017
Equivalent Diameter [µm]	6.554 ± 1.212	6.325 ± 1.039	< 0.001
Circumference [µm]	22.370 ± 4.327	21.629 ± 3.606	0.0236
Formfactor	0.911 ± 0.078	0.892 ± 0.087	< 0.001
MinFeret [µm]	5.870 ± 1.218	5.534 ± 1.111	< 0.001
MaxFeret [µm]	8.474 ± 1.719	8.361 ± 1.541	0.934
MaxFeret90 [µm]	6.206 ± 1.290	5.912 ± 1.212	0.0016
Density	241.850 ± 170.354	338.241 ± 384.209	< 0.001

3.5. Correlation Between Morphometry and Molecular Data

To evaluate the relationship between proliferation and nuclear pleomorphism, results of Ki-67-index and p53 immunoreactivity were compared with morphometry parameters (NACV, Nuclear Area and TMB) (see Table 2).

Table 2. The Ki-67-Index in NRTs (mean 4.3%) was generally lower than in RCs (overall mean 6.5%). Primary tumors of recurrent cases showed Ki67 levels comparable to NRTs (mean 4.1%), whereas the last available long-term recurrences showed higher proliferation (mean 7.1%). Across all four recurrent cases, the Ki-67 index increased by a mean of 5.9% from primary tumor to last recurrence. p53 positivity behaves similarly to Ki-67 in case 8 with a significant increase in the recurrences as compared to the primary tumor. The remaining recurrent showed low or absent p53 immunoreactivity. Only two samples exceeded the predefined 53-high threshold (>10% positive tumor nuclei).. Intriguingly, in NRTs the change in mean nuclear area over time corelated with the percentage share of p53 positive nuclei and reflected the pleomorphic pattern change. TMB did not show uniform longitudinal changes across recurrent cases. However, the overall mean TMB of NRTs (1.55) was lower than in RCs (4.71) but did not reach statistical significance (Mann-Whitney U, p = 0.052). n.s. = not sequenced.

NRT/ Recurrent Case	Case No.	Ki-67-Index [%]	p53 [%]	NACV	TMB
NRTs	1	4.18	2.51	31.83	0.41
	2	10.68	10.01	35.47	0.68
	3	7.53	7.43	30.32	0.09
	4	0.44	2.57	24.51	0.38
	5	2.82	24.13	24.71	0.18
	6	2.09	0.00	35.10	0.21
	7	1.67	0.17	53.43	0.12
	12	7.12	0.00	37.09	10.35
Recurrent Case 8	C8_P (primary)	1.68	0.00	30.79	0.76
	C8_R1 (first recurrence)	2.78	14.14	26.11	0.18
	C8_R2 (second recurrence)	6.38	11.21	23.33	1.71

 doi:10.20944/preprints202602.0214.v1

	C8_R3 (third recurrence)	7.28	11.32	22.59	2.91
	C8_R4 (fourth recurrence)	8.98	24.98	41.54	3.44
Recurrent Case 9	C9_P (primary)	7.62	0.00	31.05	1.88
	C9_R1 (first recurrence)	3.26	0.31	33.97	8.44
	C9_R2 (second recurrence)	9.01	0.00	40.67	n.s.
	C9_R3 (third recurrence)	8.85	0.00	27.74	12.62
	C9_R4 (fourth recurrence)	7.05	0.00	49.89	0.97
Recurrent Case 10	C10_P (primary)	9.96	7.10	25.99	0.06
	C10_R1 (first recurrence)	0.08	0.01	25.78	n.s.
	C10_R2 (second recurrence)	14.69	3.45	31.44	13.88
Recurrent Case 11	C11_P (primary)	0.18	0.00	17.90	n.s.
	C11_R1 (first recurrence)	4.88	0.00	26.59	7.53
	C11_R2 (second recurrence)	9.25	0.00	27.46	8.56
	C11_R3 (third recurrence)	9.30	0.00	32.10	3.65

Samples were stratified into Ki-67-low (<5%) and -high (>5%) groups and mean nuclear area was compared between groups using the Mann-Whitney-U-Test. As shown in Table 3, the mean nuclear area in the Ki-67-high group (35.96 µm²) was larger compared to the Ki-67-low group (31.76 µm²). However, Mann-Whitney-U test showed a p-value of 0.085, which may reflect limited power given the sample size (Table 3). Analogously, samples were stratified into p53-high (> 10% positive nuclei) and p53-low (< 10%). As shown in Figure 4, half of the NRTs and all recurrences of case 8 stained strongly positively. p53-high samples had a higher mean nuclear area (36.42 µm²) than the p53-negative group (33.42 µm²), although results remained statistically non-significant (p=0.15). Nuclear area did not differ significantly between samples with high versus low TMB. Furthermore, samples with high proliferation indices or high p53-positivity did not show a significantly higher tumor mutational burden.

Table 3. All samples were stratified into Ki-67-, p53-, and TMB-high and low groups. The cut-offs for the high-group were respectively: Ki-67 > 5%, p53 staining > 10% and TMB > 6.5 Mut/Mb. The Ki-67-high group had a higher mean nuclear area as compared to the low group as well as a slightly higher TMB. Samples with higher p53 positivity also had a higher mean nuclear area but lower tumor mutational burden. However, none of the results were statistically significant as tested through Mann-Whitney-U. Samples with high TMB did not differ in nuclear area from samples with low TMB.

Measurement		Mean Measurement	Mean Nuclear Area [µm]	p	TMB	p
Ki-67-index	low	2.19% (n=10)	31.76	0.085	2.93 (n=8)	0.142
	high	8.62% (n=15)	35.96		4.37 (n=14)	
p53 positivity	low	1.27% (n=19)	33.42	0.155	4.37 (n=16)	0.438
	high	15.97% (n=6)	36.31		1.51 (n=6)	
TMB	low	1.13 Mut/Mb (n=16)	34.08	0.531	-	-
	high	10.23 Mut/Mb (n=6)	35.04		-	

When plotted against the elapsed time between the primary tumor and subsequent recurrences, Ki-67 indices and mean nuclear area showed similar trajectories (Figure 8), consistent with the preceding comparisons.

 doi:10.20944/preprints202602.0214.v1

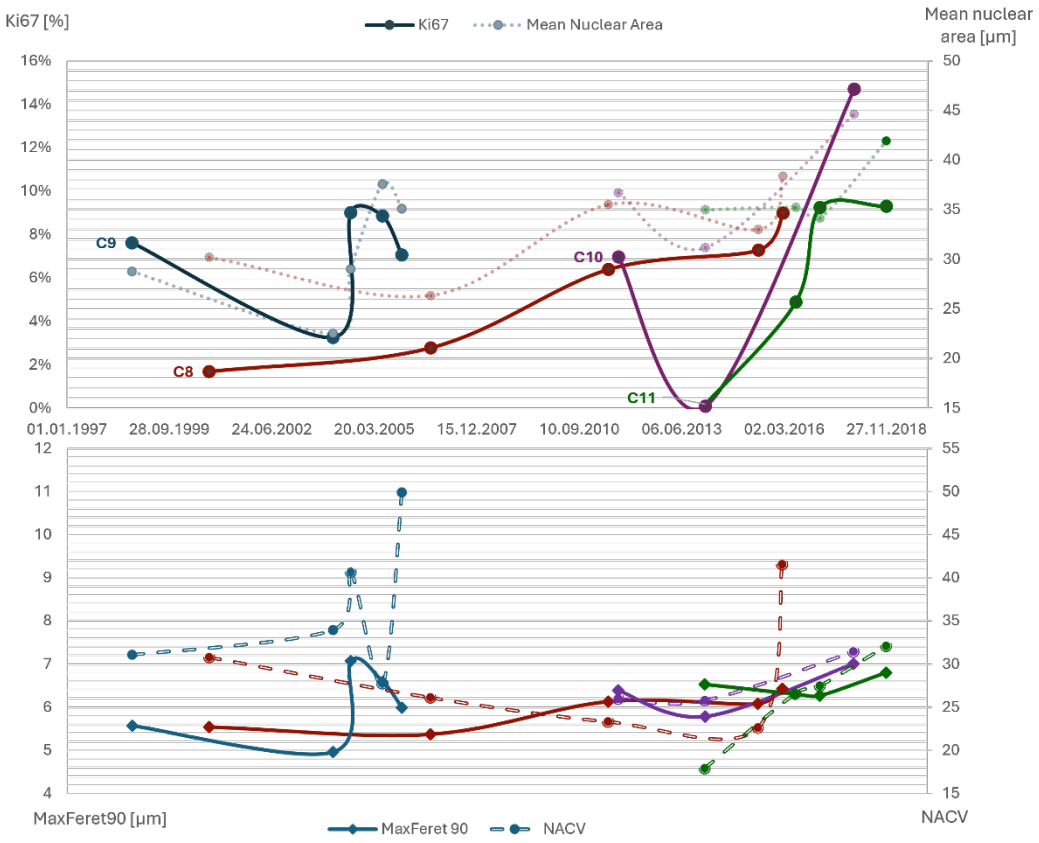

Figure 8. Correlation of the development of Ki-67-index with mean nuclear area as well as MaxFeret90 with the NACV over the exact timeline of recurrence evolution in all four recurring cases. Nuclear pleomorphic parameters correlate well with the relative proliferative activity over time in all recurrence cases.

The coefficient of variation of nuclear area (NACV) reflects heterogeneity in nuclear size and correlated well with asymmetry-related measures as represented through MaxFeret90. Both parameters showed analogical progression with a tendence towards higher NACV and MaxFeret90 over time. A high NACV reflects greater variability in nuclear size while an increased MaxFerret90 indicates elongated and irregular nuclear shape. Taken together, these parameters are proficient quantitative markers of nuclear pleomorphism.

Analysis of TMB and the mutational spectrum (Figure 9 a) did not show obvious differences between NRTs, primary tumors from recurrent cases and long-term recurrences or metastases. The mean TMB in long-term recurrences (4.75 Mut/Mb) was significantly ($p = 0.02$ via Mann-Whitney U) higher than the mean TMB of NRTs (1.55 Mut/Mb). A detailed examination of the mutational spectrum (Fig 9 b) revealed a consistent ratio of InDels to SNVs found in all samples. This reproducibility across independent sequencing runs and experimental batches supports the internal consistency of the variant-calling workflow and provides an additional, qualitative measure of internal quality control. Closer examination of SNVs showed a missense-dominated mutational composition. A transition-transversion plot was used for further characterization of the SNV spectrum observed across this dataset. The VENN-diagram in Figure 8c indicates a modest number of shared mutations throughout serial long-term recurrences of the same patient.

 doi:10.20944/preprints202602.0214.v1

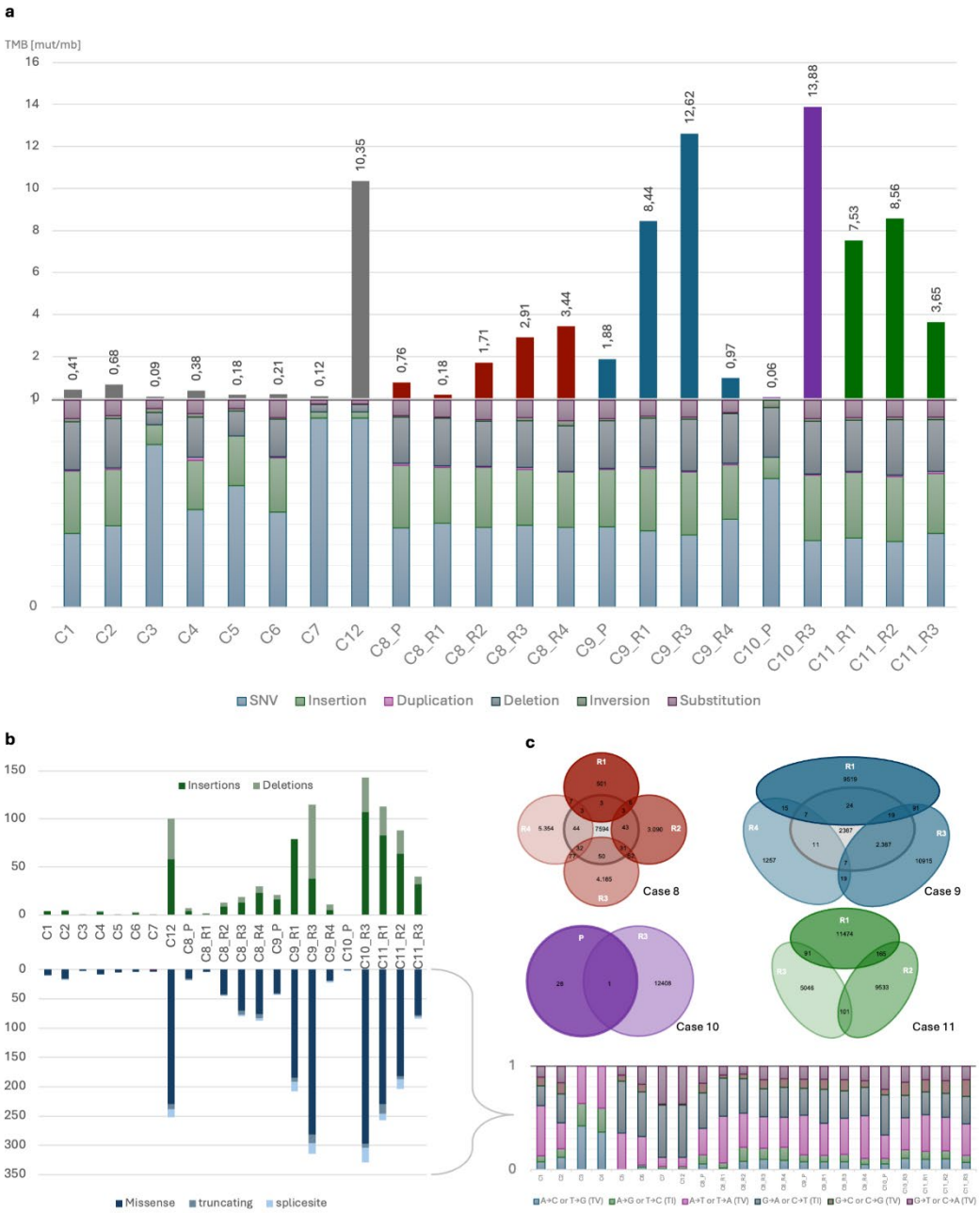

Figure 9. (a) Correlation of tumor mutational burden (TMB) with the mutational distribution of all samples. With the exemption of case 12 all NRTs displayed a lower TMB than long-term recurrences or metastases of RCs. The mean TMB in recurrent cases (4.75 Mut/Mb) was significantly ($p = 0.02$ via Mann-Whitney U) higher than the mean TMB of NRTs (1.55 Mut/Mb). Case 8 showed a continuous increase in TMB throughout its re-currences whereas no trend could be observed in other RCs. Mutational events were predominantly represented by single-nucleotide variants (SNVs) and insertions as well as deletions (InDels). (b) Insertions occurred more frequently than deletions. SNVs were dominated by missense mutations. The Transitions (TI) and Transversions (TV) graph summarized the spectrum of SNVs detected in this dataset. Substitutions within the same nucleotide class are classified as Transitions (TI), substitutions between nu-cleotide classes are transversions (TV). (c) VENN-Diagram of all mutations found within the recurrent cases before filtering, highlighting their shared mutations (classified as alterations with the same amino acid change at the same position).

4. Discussion

 doi:10.20944/preprints202602.0214.v1

Chordomas are rare malignant tumors of the axial skeleton with high recurrence rates despite their low-grade histological appearance [47]. Reliable prognostic markers for identifying patients at risk of recurrence remain scarce, complicating therapeutic stratification and follow-up [48–51].

In recent years, morphometric analysis of nuclear features has emerged as a promising tool for assessing tumor behavior across various cancer types [17,18]. By quantifying subtle changes in nuclear size, shape and density, these techniques may capture histological correlates of biological aggressiveness that are not readily apparent on routine microscopy [52]. Histologically, abnormalities of the cellular nucleus have been a pivotal criterion for the histopathologic diagnosis of malignancy [9,28], automatically taking aspects of size, shape, chromatin structure and particularly irregularities of the outer nuclear membrane into consideration [29,30]. Several studies have demonstrated that nuclear morphometric alterations may distinguish aggressive tumor behavior, including metastatic potential or recurrence in other malignancies [22–25,42]. Despite these promising findings, such approaches have not yet been applied systematically to chordoma [43].

To investigate whether nuclear pleomorphic changes are associated with tumor progression in chordoma, we quantified nuclear features through nuclear morphometry and integrated these data with immunohistochemical findings and tumor mutational burden derived from whole exome sequencing. This study addressed the following questions:

1. Do non-recurrent tumors exhibit significant differences in morphometric parameters?
2. Do tumors with multiple long-term recurrences and/or metastases show measurable changes in pleomorphism over time and do levels of lamin A/C, which are key filament proteins of the nuclear envelope changer correspondingly?
3. Do primary tumors from patients who later recur differ from non-recurrent tumors at baseline?
4. Are nuclear morphometric changes associated with molecular measures of mutational load, particularly TMB?

Our analysis of non-recurrent tumors (NRTs) revealed considerable intertumoral variability in nuclear morphology. Approximately 80% of all comparisons across size, shape, and density parameters demonstrated statistically significant differences between samples. Chordomas are known for pronounced intratumoral heterogeneity, which may be reflected even within morphologically stable cases or reflect different clonal regions with variable morphometric profiles [53,54]. To minimize sampling bias, multiple regions per tumor were chosen at random and analyzed. Nonetheless, the observed variability may reflect biological differences in tumor cell populations, anatomical site-specific factors or early stage subclonal diversification that does not necessarily result in recurrence. These results highlight the need to contextualize morphometric features within the overall tumor architecture and to interpret single-parameter readouts cautiously when considering morphometry for risk assessment.

In tumors from patients with multiple long-term recurrences, we observed consistent and statistically significant changes over time. Most notably, size related parameters, including nuclear area, equivalent diameter and circumference, tended to increase across successive recurrences. These changes were paralleled by evolving asymmetry in nuclear shape, reflected in altered formfactor and ferret-based measurements. These morphometry transformations may reflect changes in clinical presentation, phenotypic shifts and progressive disease evolution as well as an increase in genomic instability. Furthermore, increasing NACV across recurrences supports nuclear pleomorphism as a quantitative morphological correlate of tumor heterogeneity and potentially aggressive behavior [8]. As important components of the nuclear envelope nuclear lamins play a central role in cancer development and are crucial for the mechanics and shape of the nucleus [55–57]. They are correlated with cytologic malignancy criteria and are involved in cancer progression [58]. Lamin A plays a pivotal role in maintaining morphological nuclear structure in ovarian cancer [59]. Loss of lamin A/C is associated with metastasis and poor prognosis in breast cancer as well as poor differentiation in gastric cancer [60–62]. Correspondingly we observed a negative correlation between lamin A/C expression in the nuclear envelope and shape as well as size parameters. A similar inverse correlation has previously been described in Ewings sarcoma [63]. Furthermore, pleomorphic nuclei in the last

 doi:10.20944/preprints202602.0214.v1

recurrence revealed abnormal cytoplasmic localization of the lamin A/C component with only lamin-remnants remaining in the nuclear envelope. This spatial disintegration correlated with the increased nuclear pleomorphism over time proving that lamin A/C provides mechanic stability as central intermediar filaments of the nuclear envelope. In line with recent literature, the abnormal localization of lamins suggests a causal role in tumor progression through facilitation of pleomorphic nuclear development, confirming a direct relation between morphometric nuclear alterations and the molecular integrity of nuclear envelope components [64].

Overall, these findings suggest that recurrence evolution is accompanied by measurable nuclear remodeling, offering a morphological window into biological shifts that drive disease progression. Among the recurrent cases, patient 10 stood out due to the development of multiple hematogenous metastases over seven years. The clinical course is compatible with a particularly aggressive disease phenotype, potentially reflecting unique tumor biology or patient specific risk factors [65]. In this patient we observed the largest rise in TMB across serial samples and highest Ki-67 index in a metastatic lesion (14.7%), together with pronounced morphometric changes, supporting the hypothesis that advanced disease may be associated with accelerated proliferation, measurable nuclear remodeling and molecular changes. Furthermore, this may indicate a higher degree of malignancy in long-term hematogenous metastatic chordoma tissue compared with local recurrences. A similar phenomenon has been reported in long-term metastases of breast cancer [33].

However, given the small cohort size, these observations remain hypothesis-generating and require confirmation in larger cohorts of metastatic chordoma. Despite the marked clinical divergence, radiological assessment did not reveal consistent distinguishing features, highlighting the limitations of conventional imaging techniques in predicting tumor behavior [47,66] and reinforcing the potential value of quantitative nuclear profiling to identify aggressive trajectories.

Primary tumors from patients who later developed multiple long-term recurrences differed significantly from non-recurrent tumors in several morphometric parameters. They exhibited smaller nuclei with greater asymmetry and higher density. These quantitative features were not apparent through conventional histological evaluation, underscoring the added diagnostic value of morphometric analysis. The increased nuclear density observed in primary tumors may reflect denser chromatin packaging, increased DNA content or altered transcriptional activity – features often associated with biological aggressiveness in other malignancies [67]. One possible explanation for the observed smaller nuclei is that these tumors may harbor subclonal populations with highly compacted chromatin [58], resulting in reduced nuclear size despite increased functional activity [68]. Alternatively, smaller nuclei with irregular contours could reflect a distinct differentiation state predisposing these tumors to recurrence [28]. Similar morphometric patterns have been reported in prostate and thyroid carcinomas, where smaller, denser nuclei with higher asymmetry, were associated with adverse outcomes despite their otherwise low histological grade [15,28,42]. Altogether, these findings suggest that morphometric indicators of more aggressive behavior and recurrence potential may already be present at the time of initial diagnosis, offering a possible avenue for earlier risk stratification.

Taken together, the morphometric and immunohistochemical findings point toward progressive biological transformation in recurrent chordomas. The increase in nuclear size, asymmetry and density over time, as seen in Figure 7, was paralleled by higher Ki-67 indices in recurrent tumors, suggesting a shift toward a more proliferative phenotype. [69–71]. Several cases exhibited additional immunohistochemical alterations: Case 8 showed increased p53 expression and partial loss of SMARCB1, potentially indicating impaired chromatin remodeling and tumor suppressor function. SMARCB1 loss over time, as observed in case 8, and reduced expression across all recurrent cases, has previously been associated with poorly differentiated chordomas and could indicate epigenetic dysregulation in more aggressive subtypes [45,46]. However, Maioli et al. found mosaic or clonal partial loss of SMARCB1 in conventional spinal chordoma which could explain weak staining or loss of expression within NRTs [46]. Case 11 gained positivity for brachyury, VEGF, EGFR and S100 while case 9 gained EGFR-Expression as well and case 10 showed increased expression of p53 in its

 doi:10.20944/preprints202602.0214.v1

metastatic lesions. Stronger VEGF, EGFR and S100 staining in recurrences further suggests involvement of angiogenic differentiation pathways during tumor evolution. VEGFA-Expression has previously been associated with shorter progression free survival underlining our finding of increased expression over time in three out of four recurrent cases [72]. E-cadherin expression was negative in all samples hinting at a chordoma-typical mesenchymal switch profile with upregulation of N-cadherin and downregulation of E-cadherin which could be caused by repression of CDH1 through promoter methylation. Consistent with prior observations in conventional chordoma, PD-L1 and PD-1 were negative in most patients as well (0% / 17%) suggesting a limited role of these markers in the immune microenvironment of chordoma [73]. However, the diversity in staining patterns across cases suggests that chordoma recurrence is not driven by a uniform set of molecular events, but rather by heterogenous biological trajectories [29,74]. Integration of pleomorphic changes with immunohistochemical findings, such as the significantly increased Ki-67 index in the recurrences, altered p53 expression patterns and partial loss of SMARCB1, supports the interpretation that recurrent-stage tumors display higher proliferative activity with potentially increased genetic instability [28,75,76]. These findings reinforce the value of nuclear morphometry as a reproductible and quantifiable tool, that captures biologically relevant changes even in the absence of consistent immunohistochemical alterations.

Morphonuclear profiling in long-term recurrences was integrated with tumor mutational burden (TMB) as a measure of molecular genetic complexity. TMB is defined as the total number of somatic nonsynonymous mutations present within the exome of the cancer genome [75]. In clinical oncology it is used to predict the response to immune checkpoint therapy [77,78] but can be used as a measure of the molecular genetic complexity of malignant tumors as well [79]. Literature shows that nuclear morphology is associated with metrics of genomic instability in multiple cancer types [19]. The relationship between TMB and nuclear morphology is substantiated by several investigations describing the possibility of predicting tumor mutational burden from histopathological images, for example in lung adenocarcinoma [80] and colorectal cancer [81,82]. Samples of patients without recurrences showed a significantly lower TMB than samples of recurrent cases ($p = 0.02$). TMB in Chordoma has been reported as generally low with a range of 0.05-7.68 mut/mb [83], but studies investigated only one recurrence paired with their primary tumor. On average, recurrence samples showed increased number of SNVs (30.1% higher), indels (43.1% higher), genomic regions covered by SCNAs (2.1% higher), and SVs (43.5% higher), compared with the matched primary tumor samples. The time to the first recurrence (TTFR) ranged from 3 to 36 months with a median of 8 months excluding long-term recurrences. Investigations into TMB of other solid tumors yielded different results: An average tumor mutational burden in triple negative breast cancer of 7.6 mut/mb was observed with 8.3 mut/mb in recurrent tumors and 7.2 mut/mb in primary tumors that did not recur [84]. Contrarily, Wei et al found a positive correlation between time of relapse and increased TMB in glioblastomas [53]. Metastatic tumors are pathogenetically related but differ from recurrent tumors and should be assed differently. In non-small cell lung cancer, the molecular genetic pattern of brain metastases differed from primary tumors [85].

In our study, TMB varied between patients throughout the development of long-term recurrences and metastases over a time span of seven to 16 years. Several investigations have shown that TMB can differ between primary tumors and recurrences [86]. A comprehensive genome-wide comparison of primary and metastatic solid tumors reported that the majority of cancer types exhibited either moderate genomic variations (e.g., lung adenocarcinoma) or relatively conserved genomic patterns (e.g., ovarian serous carcinoma) [87]. The same study also described global genomic differences between primary and metastatic cancers: metastatic tumors often showed higher clonality and lower intratumor heterogeneity than primary tumors. Overall, these findings suggest that TMB alone does not necessarily indicate tumor progression. Tumor progression is more closely linked to clinically relevant driver genes.

In our cohort of long-term recurrent chordomas, nuclear morphometric parameters including size and shape factors showed statistically significant changes over time. Although these alterations

 doi:10.20944/preprints202602.0214.v1

were moderate in absolutes, they reflected a morphometric nuclear development over time of recurrences and correlated well with decreasing lamin A/C expression, which may contribute to reduced nuclear mechanical stability. The inverse correlation of lamin A/C expression at the nuclear envelope and nuclear area/shape parameters offers a plausible mechanistic link between the observed increase in nuclear irregularity and the higher proportion of pleomorphic nuclei in recurrences. This is compatible with the overall modest molecular evolution captured by TMB. To our knowledge, no other studies have integrated longitudinal quantitative morphometry with genomic profiling in long-term recurrent/metastatic chordoma. Our comparative analysis provides exploratory evidence linking morphonuclear changes with molecular features in long-term recurrences and metastases. These findings may contribute to a better understanding of recurrence formation and metastasis in chordoma and inform future studies aimed at biomarker-guided stratification and therapeutic development.

Semiautomated methods – typically involving manual tracing of nuclei on digitalized histologic images – have long been a standard approach in the assessment of nuclear morphometry [37]. While fully automated image analysis pipelines are not yet standard in routine histopathology, advances in artificial intelligence (AI) and digital pathology are expected to accelerate their adoption in the near future [88,89]. As manual tracing of nuclei for morphometry analysis would be too time-consuming in a diagnostical clinical setting and may introduce observer-dependent variability, the rapid progress in AI-programs could improve the possibilities for quantitative and qualitative nuclear assessment and contribute to more reliable cancer diagnostics [90]. Observer variability was mitigated in our study by using a single trained investigator for all measurements who was blinded to sampling status and patient data. This study could provide data on nuclear development in long-term recurrences and tracing results could be used as a training base for future AI-based studies due to the high number of measurements taken per sample.

5. Conclusions

In this study quantitative nuclear morphometry captured measurable phenotypic remodeling during long-term recurrence evolution and metastasis. Non-recurrent chordomas showed substantial intertumoral variability, whereas serial samples from recurrent/metastatic cases demonstrated consistent longitudinal changes, most predominantly in size- and shape-related parameters, accompanied by higher proliferative activity in recurrent lesions. Notably, primary tumors from patients who later recurred differed from non-recurrent tumors in several morphometry features despite comparable qualitative histology, suggesting that recurrence-prone phenotypes may already be detectable at initial diagnosis using quantitative nuclear profiling.

Integration of morphology with immunohistochemistry and whole-exome sequencing indicated that morphonuclear remodeling occurs alongside heterogeneous molecular trajectories. TMB remained overall low but varied across patients and timepoints and was higher in recurrent tumors, emphasizing that mutational load alone is not a uniform surrogate of progression in chordoma. Lamin A/C expression decreased throughout time within the recurrences and was inversely associated with nuclear irregularity, providing a mechanistic link between loss of nuclear envelope integrity and increased pleomorphism.

Collectively, these data support nuclear morphometry complemented by immunophenotypic and next-generation sequencing (NGS) as a quantitative adjunct to routine evaluation. They may be a foundation for future, larger cohorts to validate patient-level predictive AI models and relate morphonuclear remodeling to driver events and therapeutic vulnerabilities in long-term recurrent and metastatic chordoma.

Author Contributions: Conceptualization, A.R. and S.R.U.; methodology, S.R.U., A.R.; software, S.R.U., J.M.U., J.S.; validation, A.R., J.C.A.U.C. and F.K.; formal analysis, S.R.U.; investigation, S.R.U.; resources, A.R., C.L., M.R., D.S., M.G., S.F.; data curation, S.R.U., J.S.; writing—original draft preparation, S.R.U.; writing—review and editing, S.R.U., A.R., J.S., J.C.A.U.C., M.G, F.K.; visualization, S.R.U., J.M.U.; supervision, A.R.; project

 doi:10.20944/preprints202602.0214.v1

administration, A.R.; funding acquisition, A.R. All authors have read and agreed to the published version of the manuscript.

Funding: This research received no external funding.

Institutional Review Board Statement: The study was conducted in accordance with the Declaration of Helsinki and approved by the Ethics Committee of the medical faculty of the Otto-von-Guericke-University of Magdeburg, Germany (protocol code 132/21).

Informed Consent Statement: Patient consent was waived due to the retrospective aspect of the study. Paraffine embedded archive material, from patients who are no longer alive, was collected over decades and consent was obtained through the Ethics Committee protocol code 132/21 (see above).

Data Availability Statement: The original contributions presented in this study are included in the article/supplementary material. Further inquiries can be directed to the corresponding authors. The raw data supporting the conclusions of this article will be made available by the authors on request.

Conflicts of Interest: The authors declare no conflicts of interest.

Abbreviations

The following abbreviations are used in this manuscript:

AI	Artificial Intelligence
AltAF-index	Alternate Allele Friction index
BNCT	Benign Notochordal Cell Tumor
dbSNP	Single Nucleotide Polymorphism Database
DNA	Deoxyribonucleic acid
EDTA	Ethylenediaminetetraacetic acid
EGFR	Epidermal Growth Factor Receptor
FFPE	Formalin-fixed paraffin-embedded
GRCh37	Genome Reference Consortium Human Build 37
H&E	Hematoxylin and Eosin
InDel(s)	Insertion(s) and Deletion(s)
Ki-67	Ki-67 proliferation index
MAF	Minor Allele Frequency
MATLAB	Matrix Laboratory (MathWorks software)
MaxFeret	Maximum Feret diameter
MaxFeret90	Maximum Feret diameter measured at 90° rotation
Mb(s)	Megabase(s)
MinFeret	Minimum Feret diameter
Mut/Mb	Mutations per Megabase
NACV	Nuclear Area Coefficient of Variation
NGS	Next-Generation Sequencing
NRT(s)	Non-recurrent Tumor(s)
PD-1	Programmed cell death protein 1
PD-L1	Programmed death-ligand 1
Q-Q	Quantile-quantile (plot)
RC(s)	Recurrent Case(s)
SCNA(s)	Somatic copy-number alteration(s)
SD	Standard Deviation
SMARCB1	SWI/SNF-related, matrix associated, actin-dependent regulator of chromatin, Subfamily B, Member 1
SNV(s)	Single Nucleotide Variant(s)
TMB	Tumor Mutational Burden
TTFR	Time to first Recurrence
VAF	Variant Allele Frequency
VEGF(A)	Vascular Endothelial Growth Factor (A)
WES	Whole-Exome Sequencing

 doi:10.20944/preprints202602.0214.v1

WHO World Health-Organization

Clones

The following clones were used in this study:

25/BAF47	SMARCB1 clone
315M-95	PD-1 clone
453M-95	p53 clone, DO7 designation
AE1/3	Pancytokeratin clone , PCK designation)
E30	EGFR clone
EP4520-16	Lamin A/C clone
EP700Y	E-cadherine clone
EPR18113	Brachyury clone
M3653	PD-L1 clone
MIB-1	Ki-67 clone
VG-1	VEGF clone
Vim384	Vimentin clone
Z0331	S100 antibody identifier

References

1. Karpathiou, G.; Dumollard, J.M.,. Chordomas: A review with emphasis on their pathophysiology, pathology, molecular biology, and genetics. *Pathol. Res. Pract.* **2020**, *216*, 153089.
2. Walcott, B.P.; Nahed, B.V.,. Chordoma: current concepts, management, and future directions. *Lancet Oncol.* **2012**, *13*, e69-76.
3. Antonescu, C.R. Soft tissue and bone tumours WHO Classification of Tumours Editorial Board: Cristina R. Antonescu [and 14 others], 5th edition; International Agency for Research on Cancer: Lyon, 2020, ISBN 9789283245025.
4. Barth, T.F.E.; Witzleben, A. von,. Notochordale Tumoren : Benigne notochordale Tumoren und Chordome. *Pathologe* **2018**, *39*, 117–124.
5. Cha, Y.J.; Suh, Y.L. Chordomas: Histopathological Study in View of Anatomical Location. *J. Korean Med. Sci.* **2019**, *34*, e107.
6. Casali, P.G.; Stacchiotti, S.,. Chordoma. *Curr. Opin. Oncol.* **2007**, *19*, 367–370.
7. Yamaguchi, T.; Imada, H.,. Notochordal Tumors: An Update on Molecular Pathology with Therapeutic Implications. *Surg. Pathol. Clin.* **2017**, *10*, 637–656.
8. Singh, I.; Lele, T.P. Nuclear Morphological Abnormalities in Cancer: A Search for Unifying Mechanisms. *Results Probl. Cell Differ.* **2022**, *70*, 443–467.
9. Derenzini, M.; Trerè, D.,. Nucleolar function and size in cancer cells. *Am. J. Pathol.* **1998**, *152*, 1291–1297.
10. Jairajpuri, Z.S.; Rana, S.,. Toward early diagnosis of oral cancer: Diagnostic utility of cytomorphological features, a pilot study. *Natl. J. Maxillofac. Surg.* **2019**, *10*, 20–26.
11. Horai, Y.; Kakimoto, T.,. Quantitative analysis of histopathological findings using image processing software. *J. Toxicol. Pathol.* **2017**, *30*, 351–358.
12. Girdhar, A.; Raju, K.,. Significance of Nuclear Morphometry in Breast Lesions: A Cross-Sectional Study. *Cureus* **2023**, *15*, e39378.
13. Sangwan, M.; Singh, S.,. Role of morphometry and proliferative parameters in grading of urothelial neoplasms. *Cent. European J. Urol.* **2015**, *68*, 37–44.
14. Poropatich, K.; Yang, J.C.,. Nuclear size measurement for distinguishing urothelial carcinomas from reactive urothelium on tissue sections. *Diagn. Pathol.* **2016**, *11*, 57.
15. Veltri, R.W.; Christudass, C.S. Nuclear morphometry, epigenetic changes, and clinical relevance in prostate cancer. *Adv. Exp. Med. Biol.* **2014**, *773*, 77–99.
16. Moretti, S.; Spallanzani, A.,. Correlation of Ki-67 expression in cutaneous primary melanoma with prognosis in a prospective study: different correlation according to thickness. *J. Am. Acad. Dermatol.* **2001**, *44*, 188–192.

 doi:10.20944/preprints202602.0214.v1

17. Kojima, M.; Shiokawa, A.,. Clinical significance of nuclear morphometry at the invasive front of T1 colorectal cancer and relation to expression of VEGF-A and VEGF-C. *Oncology* **2005**, *68*, 230–238.
18. Kawaguchi, K.; Kohashi, K.,. Prognostic value of nuclear morphometry in myxoid liposarcoma. *Cancer Sci.* **2023**, *114*, 2178–2188.
19. Chuang, W.-Y.; Yu, W.-H.,. Deep Learning-Based Nuclear Morphometry Reveals an Independent Prognostic Factor in Mantle Cell Lymphoma. *Am. J. Pathol.* **2022**, *192*, 1763–1778.
20. Khatri, P.; Choudhury, M.,. Role of morphometry in the cytological differentiation of benign and malignant thyroid lesions. *J. Cytol.* **2017**, *34*, 1–4.
21. Duca-Barbu, S.-A.; Bratei, A.A.,. A Novel Algorithm for Evaluating Bone Metastatic Potential of Breast Cancer through Morphometry and Computational Mathematics. *Diagnostics (Basel)* **2023**, *13*.
22. Ferguson, P.C.; Deshmukh, N.,. Change in histological grade in locally recurrent soft tissue sarcomas. *Eur. J. Cancer* **2004**, *40*, 2237–2242.
23. Wang, Z.; Lu, H.,. Predicting recurrence in osteosarcoma via a quantitative histological image classifier derived from tumour nuclear morphological features. *CAAI Trans on Intel Tech* **2023**, *8*, 836–848.
24. Hoque, A.; Lippman, S.M.,. Quantitative nuclear morphometry by image analysis for prediction of recurrence of ductal carcinoma in situ of the breast. *Cancer Epidemiol. Biomarkers Prev.* **2001**, *10*, 249–259.
25. Gearhart, J.P.; Willmann, J.R.,. Nuclear morphometric analysis of metastasis in Wilms' tumor after multimodal therapy: comparison with primary tumor. *Urology* **1995**, *45*, 119–123.
26. Naka, T.; Boltze, C.,. Skull base and nonskull base chordomas: clinicopathologic and immunohistochemical study with special reference to nuclear pleomorphism and proliferative ability. *Cancer* **2003**, *98*, 1934–1941.
27. Tauziéde-Espariat, A.; Bresson, D.,. Prognostic and Therapeutic Markers in Chordomas: A Study of 287 Tumors. *J. Neuropathol. Exp. Neurol.* **2016**, *75*, 111–120.
28. Fischer, E.G. Nuclear Morphology and the Biology of Cancer Cells. *Acta Cytol.* **2020**, *64*, 511–519.
29. Alvarado-Kristensson, M.; Rosselló, C.A. The Biology of the Nuclear Envelope and Its Implications in Cancer Biology. *Int. J. Mol. Sci.* **2019**, *20*.
30. Dey, P. Cancer nucleus: morphology and beyond. *Diagn. Cytopathol.* **2010**, *38*, 382–390.
31. Uhler, C.; Shivashankar, G.V. Nuclear Mechanopathology and Cancer Diagnosis. *Trends Cancer* **2018**, *4*, 320–331.
32. Yiong, C.S.; Lin, T.P.,. Biomarkers for immune checkpoint inhibition in sarcomas - are we close to clinical implementation? *Biomark. Res.* **2023**, *11*, 75.
33. Xu, B.; Amallraja, A.,. Case report: 16-yr life history and genomic evolution of an ER+ HER2- breast cancer. *Cold Spring Harb. Mol. Case Stud.* **2020**, *6*.
34. Gardner, P.; Bai, J.,. Editorial: Chordoma: advances in biology and clinical management. *Front. Oncol.* **2023**, *13*.
35. Koka, H.; Zhou, W.,. Genomic profiles and clinical presentation of chordoma. *Acta Neuropathol. Commun.* **2024**, *12*, 129.
36. Scheipl, S.; Igrec, J.,. Chordome: Gibt es eine molekulargenetische Grundlage für Diagnostik und Therapie? *Pathologe* **2020**, *41*, 153–162.
37. Büttner, R.; Longshore, J.W.,. Implementing TMB measurement in clinical practice: considerations on assay requirements. *ESMO Open* **2019**, *4*, e000442.
38. Budczies, J.; Kazdal, D.,. Tumour mutational burden: clinical utility, challenges and emerging improvements. *Nat. Rev. Clin. Oncol.* **2024**, *21*, 725–742.
39. Doig, K.D.; Fellowes, A.,. Tumour mutational burden: an overview for pathologists. *Pathology* **2022**, *54*, 249–253.
40. Hallermayr, A.; Neuhann, T.M.,. Highly sensitive liquid biopsy Duplex sequencing complements tissue biopsy to enhance detection of clinically relevant genetic variants. *Front. Oncol.* **2022**, *12*, 1014592.
41. Starosta, R.T.; Siebert, M.,. Histomorphometric analysis of liver biopsies of treated patients with Gaucher disease type 1. *Autops. Case Rep.* **2021**, *11*, e2021306.
42. Razavi, M.A.; Wong, J.,. Nuclear morphometry in indeterminate thyroid nodules. *Gland Surg.* **2020**, *9*, 238–244.
43. Ulici, V.; Hart, J. Chordoma. *Arch. Pathol. Lab. Med.* **2022**, *146*, 386–395.

 doi:10.20944/preprints202602.0214.v1

44. Walhart, T.A.; Vacca, B.,. SMARCB1 Loss in Poorly Differentiated Chordomas Drives Tumor Progression. *Am. J. Pathol.* **2023**, *193*, 456–473.
45. Mobley, B.C.; McKenney, J.K.,. Loss of SMARCB1/INI1 expression in poorly differentiated chordomas. *Acta Neuropathol.* **2010**, *120*, 745–753.
46. Maioli, M.; Cocchi, S.,. Conventional Spinal Chordomas: Investigation of SMARCB1/INI1 Protein Expression, Genetic Alterations in SMARCB1 Gene, and Clinicopathological Features in 89 Patients. *Cancers (Basel)* **2024**, *16*.
47. Meng, T.; Yin, H.,. Clinical features and prognostic factors of patients with chordoma in the spine: a retrospective analysis of 153 patients in a single center. *Neuro Oncol.* **2015**, *17*, 725–732.
48. Colia, V.; Stacchiotti, S. Medical treatment of advanced chordomas. *Eur. J. Cancer* **2017**, *83*, 220–228.
49. Yang, Y.; Li, Y.,. The clinical outcome of recurrent sacral chordoma with further surgical treatment. *Medicine (Baltimore)* **2018**, *97*, e13730.
50. Barber, S.M.; Sadrameli, S.S.,. Chordoma-Current Understanding and Modern Treatment Paradigms. *J. Clin. Med.* **2021**, *10*.
51. Stacchiotti, S.; Gronchi, A.,. Best practices for the management of local-regional recurrent chordoma: a position paper by the Chordoma Global Consensus Group. *Ann. Oncol.* **2017**, *28*, 1230–1242.
52. Dos Santos, J.B.; Starosta, R.T.,. Nuclear morphometry and chromatin texture changes in hepatocellular carcinoma samples may predict outcomes of liver transplanted patients. *BMC Gastroenterol.* **2022**, *22*, 189.
53. Ho, W.-M.; Chen, C.-Y.,. A longer time to relapse is associated with a larger increase in differences between paired primary and recurrent IDH wild-type glioblastomas at both the transcriptomic and genomic levels. *Acta Neuropathol. Commun.* **2024**, *12*, 77.
54. Duan, W.; Zhang, B.,. Single-cell transcriptome profiling reveals intra-tumoral heterogeneity in human chordomas. *Cancer Immunol. Immunother.* **2022**, *71*, 2185–2195.
55. Liu, S.; Yang, H.,. A snap-through instability of cell adhesion under perturbations in hydrostatic pressure. *Journal of the Mechanics and Physics of Solids* **2024**, *182*, 105476.
56. Dubik, N.; Mai, S. Lamin A/C: Function in Normal and Tumor Cells. *Cancers (Basel)* **2020**, *12*.
57. Irianto, J.; Pfeifer, C.R.,. Nuclear lamins in cancer. *Cell. Mol. Bioeng.* **2016**, *9*, 258–267.
58. Paganelli, F.; Poli, A.,. At the nucleus of cancer: how the nuclear envelope controls tumor progression. *MedComm (2020)* **2025**, *6*, e70073.
59. Watabe, S.; Kobayashi, S.,. Role of Lamin A and emerin in maintaining nuclear morphology in different subtypes of ovarian epithelial cancer. *Oncol. Lett.* **2022**, *23*, 9.
60. Bell, E.S.; Shah, P.,. Low lamin A levels enhance confined cell migration and metastatic capacity in breast cancer. *Oncogene* **2022**, *41*, 4211–4230.
61. Wu, Z.; Wu, L.,. Reduced expression of lamin A/C correlates with poor histological differentiation and prognosis in primary gastric carcinoma. *J. Exp. Clin. Cancer Res.* **2009**, *28*, 8.
62. Alhudiri, I.M.; Nolan, C.C.,. Expression of Lamin A/C in early-stage breast cancer and its prognostic value. *Breast Cancer Res. Treat.* **2019**, *174*, 661–668.
63. Chiarini, F.; Paganelli, F.,. Lamin A and the LINC complex act as potential tumor suppressors in Ewing Sarcoma. *Cell Death Dis.* **2022**, *13*, 346.
64. Kobayashi, S.; Kanehira, Y.,. Effect of lamins and emerin on nuclear morphology and histological architecture in lung adenocarcinoma. *Pathol. Res. Pract.* **2024**, *262*, 155557.
65. Zhai, Y.; Bai, J.,. Analysis of clinical factors and PDGFR-β in predicting prognosis of patients with clival chordoma. *J. Neurosurg.* **2018**, *129*, 1429–1437.
66. Sebro, R.; DeLaney, T.,. Differences in sex distribution, anatomic location and MR imaging appearance of pediatric compared to adult chordomas. *BMC Med. Imaging* **2016**, *16*, 53.
67. Streba, C.T.; Pirici, D.,. Fractal analysis differentiation of nuclear and vascular patterns in hepatocellular carcinomas and hepatic metastasis. *Rom. J. Morphol. Embryol.* **2011**, *52*, 845–854.
68. Mendaçolli, P.J.; Brianezi, G.,. Nuclear morphometry and chromatin textural characteristics of basal cell carcinoma. *An. Bras. Dermatol.* **2015**, *90*, 874–878.
69. Kashyap, A.; Jain, M.,. Role of Nuclear Morphometry in Breast Cancer and its Correlation with Cytomorphological Grading of Breast Cancer: A Study of 64 Cases. *J. Cytol.* **2018**, *35*, 41–45.

 doi:10.20944/preprints202602.0214.v1

70. Kalhan, S.; Garg, S.,. Correlation of Nuclear Morphometry with Clinicopathologic Parameters in Malignant Breast Aspirates. *South Asian J. Cancer* **2022**, *11*, 3–8.
71. Yadav, R.; Sharma, M.C.,. Prognostic value of MIB-1, p53, epidermal growth factor receptor, and INI1 in childhood chordomas. *Neuro Oncol.* **2014**, *16*, 372–381.
72. Zhai, Y.; Bai, J.,. A nomogram to predict the progression-free survival of clival chordoma. *J. Neurosurg.* **2021**, *134*, 144–152.
73. Zou, Y.; Neale, N.,. Prognostic Factors in Clival Chordomas: An Integrated Analysis of 347 Patients. *World Neurosurg.* **2018**, *118*, e375-e387.
74. Zink, D.; Fischer, A.H.,. Nuclear structure in cancer cells. *Nat. Rev. Cancer* **2004**, *4*, 677–687.
75. Denais, C.; Lammerding, J. Nuclear mechanics in cancer. *Adv. Exp. Med. Biol.* **2014**, *773*, 435–470.
76. Miller, I.; Min, M.,. Ki67 is a Graded Rather than a Binary Marker of Proliferation versus Quiescence. *Cell Rep.* **2018**, *24*, 1105-1112.e5.
77. Kalukula, Y.; Stephens, A.D.,. Mechanics and functional consequences of nuclear deformations. *Nat. Rev. Mol. Cell Biol.* **2022**, *23*, 583–602.
78. Gromeier, M.; Brown, M.C.,. Very low mutation burden is a feature of inflamed recurrent glioblastomas responsive to cancer immunotherapy. *Nat. Commun.* **2021**, *12*, 352.
79. Las Heras, J.I. de; Schirmer, E.C. The nuclear envelope and cancer: a diagnostic perspective and historical overview. *Adv. Exp. Med. Biol.* **2014**, *773*, 5–26.
80. Chalmers, Z.R.; Connelly, C.F.,. Analysis of 100,000 human cancer genomes reveals the landscape of tumor mutational burden. *Genome Med.* **2017**, *9*, 34.
81. Furtado, L.V.; Bifulco, C.,. Recommendations for Tumor Mutational Burden Assay Validation and Reporting: A Joint Consensus Recommendation of the Association for Molecular Pathology, College of American Pathologists, and Society for Immunotherapy of Cancer. *J. Mol. Diagn.* **2024**, *26*, 653–668.
82. Niu, Y.; Wang, L.,. Predicting Tumor Mutational Burden From Lung Adenocarcinoma Histopathological Images Using Deep Learning. *Front. Oncol.* **2022**, *12*, 927426.
83. Bai, J.; Shi, J.,. Gene Expression Profiling Identifies Two Chordoma Subtypes Associated with Distinct Molecular Mechanisms and Clinical Outcomes. *Clin. Cancer Res.* **2023**, *29*, 261–270.
84. Kaur, J.; Chandrashekar, D.S.,. Whole-Exome Sequencing Reveals High Mutational Concordance between Primary and Matched Recurrent Triple-Negative Breast Cancers. *Genes (Basel)* **2023**, *14*.
85. Ruíz-Patiño, A.; Zuluaga, J.,. Molecular and clonal evolution of primary lesions vs. brain metastasis in EGFR-mutated NSCLC: a retrospective cohort study. *Transl. Lung Cancer Res.* **2025**, *14*, 3824–3835.
86. Hsu, Y.-C.; Chang, Y.-H.,. Tumor mutation burden and recurrent tumors in hereditary lung cancer. *Cancer Med.* **2019**, *8*, 2179–2187.
87. Martínez-Jiménez, F.; Movasati, A.,. Pan-cancer whole-genome comparison of primary and metastatic solid tumours. *Nature* **2023**, *618*, 333–341.
88. Shimada, Y.; Okuda, S.,. Histopathological characteristics and artificial intelligence for predicting tumor mutational burden-high colorectal cancer. *J. Gastroenterol.* **2021**, *56*, 547–559.
89. Xu, Y.; Guo, J.,. Predicting rectal cancer prognosis from histopathological images and clinical information using multi-modal deep learning. *Front. Oncol.* **2024**, *14*, 1353446.
90. Abel, J.; Jain, S.,. AI powered quantification of nuclear morphology in cancers enables prediction of genome instability and prognosis. *NPJ Precis. Oncol.* **2024**, *8*, 134.